GNSS Shadow Matching: Improving Urban Positioning Accuracy Using a 3D City Model with Optimized Visibility Prediction Scoring

Lei Wang, Paul D Groves, Marek K Ziebart,
UCL Engineering, University College London, London, United Kingdom

BIOGRAPHY

All authors are members of the Space Geodesy and Navigation Laboratory (SGNL) at University College London (UCL).

Mr Lei Wang is a PhD candidate at University College London. He received a Bachelor's degree in Geodesy and Geomatics from Wuhan University in 2010. He is interested in GNSS-based positioning techniques for urban canyons. UCL and the Chinese Scholarship Council jointly fund his PhD research (lei.wang.10@ucl.ac.uk).

Dr Paul Groves is a Lecturer (academic faculty member) at UCL, where he leads a program of research into robust positioning and navigation. He joined in 2009, after 12 years of navigation systems research at DERA and QinetiQ. He is interested in all aspects of navigation and positioning, including multi-sensor integrated navigation, improving GNSS performance under challenging reception conditions, and novel positioning techniques. He is an author of about 50 technical publications, including the book *Principles of GNSS, Inertial and Multi-Sensor Integrated Navigation Systems*. He is a Fellow of the Royal Institute of Navigation and an associate editor of both *Navigation: Journal of the ION* and *IEEE Transactions on Aerospace and Electronic Systems*. He holds a BA/MA and a DPhil in physics from the University of Oxford (p.groves@ucl.ac.uk).

Prof Marek Ziebart is Professor of Space Geodesy at UCL, Vice Dean for Research in the Faculty of Engineering Science, and Director of SGNL. In 2007, *GPS World* named him as one of the 50 Leaders to Watch for his contributions to the global navigation and positioning industry. He holds a PhD in Satellite Geodesy and Astrodynamics, and is a member of the International GNSS Service Governing Board. He is a contributor to news items and documentaries on BBC Radio and Television. He has carried out numerous consultancies and research contracts, including for NASA, the US Air Force, the European Space Agency, the UK Hydrographic Office, and Ordnance Survey.

ABSTRACT

The poor performance of global navigation satellite systems (GNSS) user equipment in urban canyons is a well-known problem, especially in the cross-street direction. A new approach, shadow matching, has recently be proposed to improve the cross-street accuracy using GNSS, assisted by knowledge derived from 3D models of the buildings close to the user of navigation devices. In this work, four contributions have been made. Firstly, a new scoring scheme, a key element of the algorithm to weight candidate user locations, is proposed. The new scheme takes account of the effects of satellite signal diffraction and reflection by weighting the scores based on diffraction modelling and signal-to-noise ratio (SNR). Furthermore, an algorithm similar to k-nearest neighbours (k-NN) is developed to interpolate the position solution over an extensive grid. The process of generating this grid of building boundaries is also optimized. Finally, instead of just testing at two locations as in the earlier work, real-world GNSS data has been collected at 22 different locations in this work, providing a more comprehensive and statistical performance analysis of the new shadow-matching algorithm.

In the experimental verification, the new scoring scheme improves the cross street accuracy with an average bias of 1.61 m, with a 9.4% reduction compared to the original SS_{22} scoring scheme. Similarly, the cross street RMS is 2.86 m, a reduction of 15.3%. Using the new scoring scheme, the success rate for determining the correct side of a street is 89.3%, 3.6% better than using the previous scoring scheme; the success rate of distinguishing the footpath from a traffic lane is 63.6% of the time, 6.8% better than using the previous scoring scheme.

KEY WORDS

GNSS, Urban Canyons, 3D City Model, Shadow Matching

1. INTRODUCTION

The poor performance of global navigation satellite systems (GNSS) user equipment in urban canyons is a well-known problem in terms of both accuracy and solution availability (Jiang et al., 2011; Groves, 2011; Wang et al. 2012). In contrast, a great number of day-to-day navigation requests are made in urban areas by city residents. Advanced intelligent transportation systems, for example, rely on positioning systems for their ability to direct individual cars in order to maximize traffic flow and prioritize emergency vehicles (Bruner, J, 2008). Vehicle lane detection in lane guidance systems, location-based advertising, augmented-reality applications, and step-by-

step guidance for visually impaired and tourists all require sufficient positioning accuracy to perform their functions (Rashid et al., 2005, You et al., 2008, Broll et al., 2008). However, the availability and accuracy of GNSS in urban areas limits the use of these applications (Wang et al., 2012).
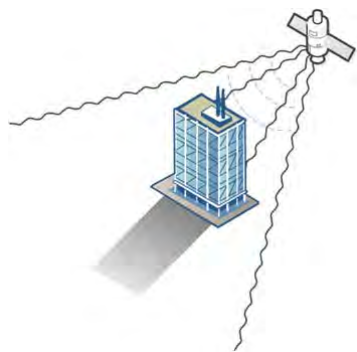

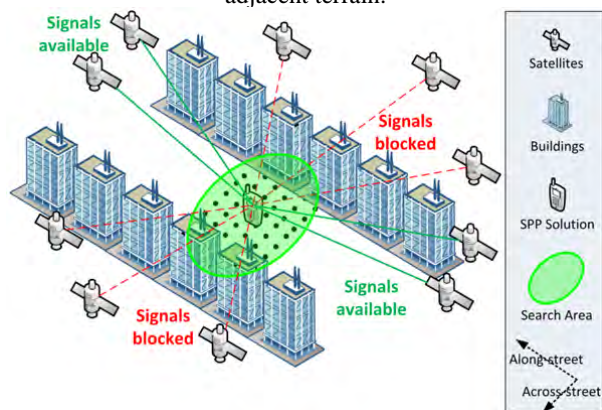Figure 1. The buildings cast GNSS shadows over the adjacent terrain.

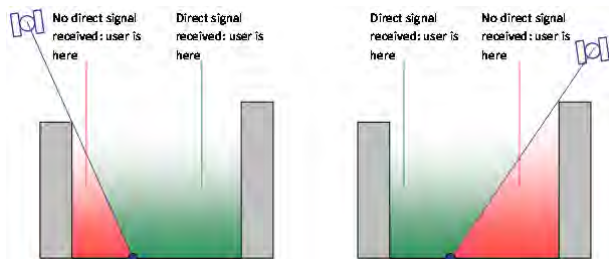Figure 2. A schematic diagram of shadow matching.

Figure 3: The shadow-matching concept: using direct signal reception to localise position

The problem of GNSS performance in urban canyons arises because where there are tall buildings or narrow streets, the direct line-of-sight (LOS) signals from many, sometimes most, of the satellites are blocked. The buildings effectively cast GNSS shadows over the adjacent terrain. Figure 1 illustrates this. Without direct signals from four or more satellites, an accurate position solution cannot be determined. Sometimes, a degraded position solution may be obtained by making use of signals that can only be received by reflection off a building; these are known as non-line-of-sight (NLOS) signals (Ercek et al., 2005; Viandier et al., 2008).

As well as affecting the number of available GNSS signals, an urban canyon also affects the geometry of satellites, which causes lower accuracy in the cross-street direction. This is because signals with lines of sight going across the street are much more likely to be blocked by buildings than signals with lines of sight going along the street. This is illustrated by Figure 2. As a result, the signal geometry, and hence the positioning accuracy, will be much better along the direction of the street than across the street (Groves, 2011).

For improving navigation performance in highly built-up areas, a variety of navigation sensors have been used to enhance or augment GNSS. Road vehicles typically combine GNSS with odometers, and map-matching algorithms, while pedestrian navigation users may combine GNSS with cell phone signals, Wi-Fi and/or dead reckoning using inertial sensors, magnetic compass and barometric altimeter (Groves, 2008; Farrell, 2008). However, these approaches improve the continuity and robustness of the position solution, but not the cross-street accuracy.

A new approach has recently be proposed to improve the cross-street accuracy using GNSS, assisted by knowledge derived from 3D building models close to the user of navigation devices (Groves, 2011). As 3D building models are becoming more accurate and widely available (Bradbury, 2007; Bradbury et al., 2007), they may be treated as a new data source for urban navigation and used to improve cross-track positioning accuracy in urban canyons. This can be achieved by predicting which satellites are visible from different locations and comparing this with the measured satellite visibility to determine position. Satellite visibility predictions using a 3D city model have been validated with real-world observation, demonstrating the practical potential of shadow matching (Bradbury, 2007; Bradbury et al., 2007; Suh and Shibasaki, 2007; Kim et al., 2009; Ji et al., 2010; Wang et al, 2012). A preliminary shadow-matching algorithm has been developed and demonstrated the ability to distinguish pavement from vehicle lane, and identify the correct side of street using real-world GPS and GLONASS measurements (Wang et al, 2011, Groves et al., 2012).

However, only direct line-of-sight (LOS) signals are predicted in the earlier algorithm, whereas the user equipment can also observe diffracted and reflected signals. This mismatch can degrade shadow-matching performance. In this work, four contributions have been made. Firstly, a new scoring scheme, a key element of the algorithm to weight candidate user locations, is proposed. The new scheme takes account of the effects of satellite signal diffraction and reflection by weighting the scores based on diffraction modelling and signal-to-noise ratio (SNR). Furthermore, an algorithm similar to k-nearest neighbours (k-NN) is developed to interpolate the position solution over an extensive grid. The process of generating this grid of building boundaries is also optimized. Finally, instead of just testing at two locations as in the earlier work, real-

world GNSS data has been collected at 22 different locations in this work, providing a more comprehensive and statistical performance analysis of the new shadow-matching algorithm.

The improved shadow-matching algorithm is described in Section 2, employing a set of new scoring schemes to acknowledge signal diffraction and reflection. Section 3 then describes the testing of the algorithm using real-world GPS and GLONASS measurements, and compares performance of the shadow-matching algorithm using different scoring schemes. Finally, in Section 4, conclusions are drawn and future work discussed.

2. SHADOW MATCHING OPTIMIZATION

This section describes the full implementation of the shadow-matching algorithm and discusses how it was optimized. Section 2.1 first explains the existing shadow-matching algorithm. Section 2.2 then gives a comprehensive implementation of the algorithm, which consists of two phases – offline phase and online phase. Each step in the two phases are further introduced, with emphasis on optimization in grid generation of building boundaries and a set of proposed new scoring schemes.

2.1 The Existing Shadow-matching Algorithm

The principle of shadow matching is simple (Groves, 2011). Due to obstruction by buildings in urban canyons, signals from many GNSS satellites will be receivable in some parts of a street, but not others. Figure 3 illustrates this, noting that the boundary between the two regions is fuzzy due to diffraction effects at building edges (Bradbury, 2007). Where each direct signal is receivable can be predicted using a 3D city model. Consequently, by determining whether a direct signal is being received from a given satellite, the user can localise their position to within one of two areas of the street. By considering other satellites, the position solution may be refined further. At each epoch, a set of candidate user positions is generated close to the user's low-accuracy conventional GNSS positioning solution. At each candidate user position, the predicted satellite visibility is matched with the real observations. The candidate position that has the best match between the prediction and the real observations is deemed the shadow matching positioning solution. This process can be conducted epoch by epoch, so the GNSS user can be either static or dynamic. Figure 2 illustrates this process.

2.2 The Improved Shadow-matching Algorithm

The new shadow-matching algorithm has two phases – the offline phase (the preparation step) and the online phase, consists of five steps, both illustrated in Figure 4. An off-line phase is conducted to generate a grid of building boundaries. In the beginning of the online phase, the user position is first initialized, e.g. using standard point positioning (SPP) with GNSS pseudo-ranges. The second step defines the search area for the shadow-matching position solution. For the third step, the satellite visibility at each grid position is predicted using the building boundaries generated from the 3D city model. After that, the similarity of satellite visibility between prediction and observation is evaluated using a scoring scheme, providing a score for each grid point in search area. Finally, the shadow-matching positioning solution is generated by a modified k-nearest neighbours algorithm, which averages the grid points with the highest scores. Each of the steps is described in more detail below.
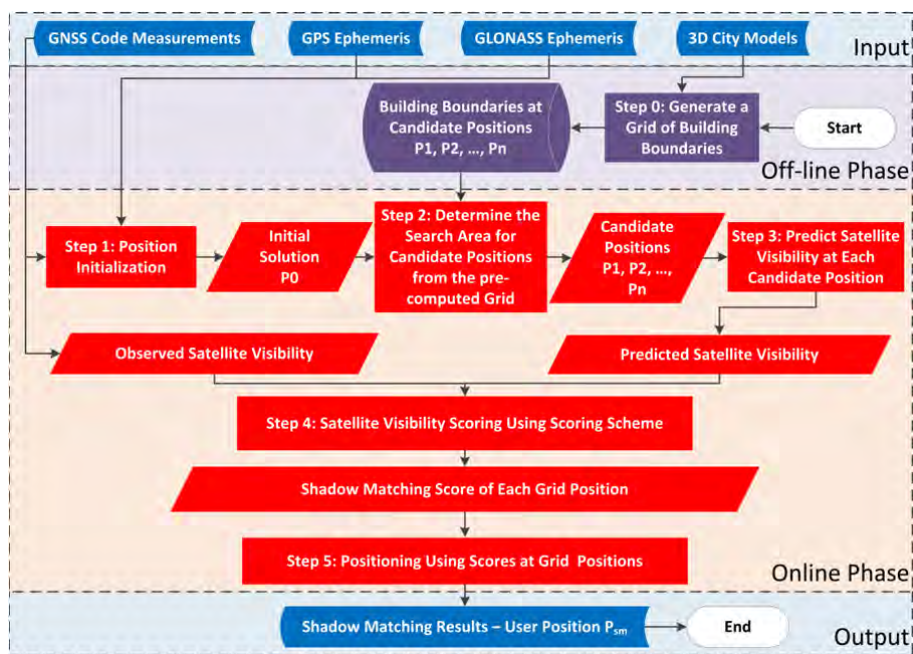

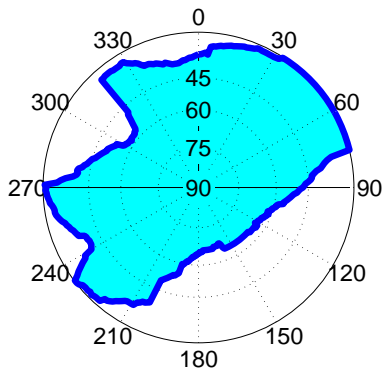Figure 4: A workflow of the improved shadow-matching algorithm.

Figure 5: An example of a building boundary as azimuth-elevation pairs in a sky plot. (The centre of the plot correspond to a 90º elevation or normal incidence)
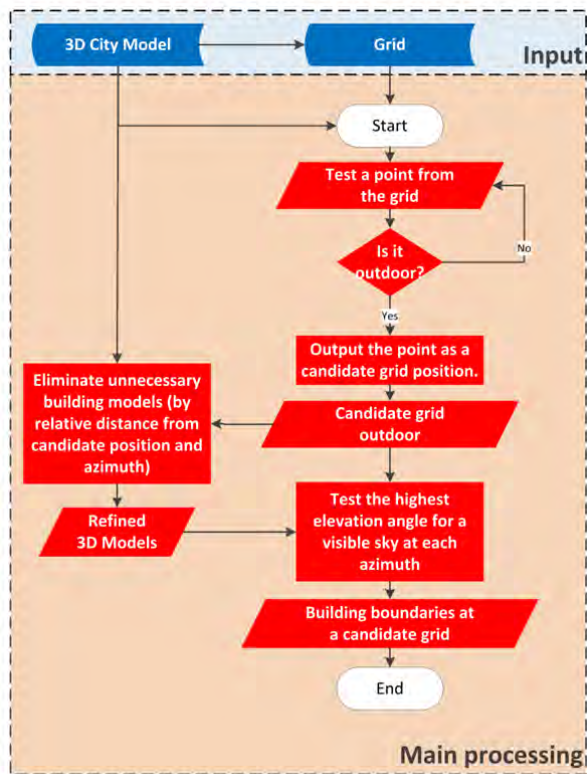

Figure 6: The process generating the grid of building boundaries

- Step 0: Generate a Grid of Building Boundaries

In the off-line phase, building boundaries at a grid of locations are generated. A building boundary means from a GNSS user's perspective, the building's edge determined for each azimuth (from 0 to 360°) as a series of elevation angles. The results from this step show where the building edges are located within an azimuth-elevation sky plot. Figure 5 shows an example of a building boundary computed from a candidate user location. Once the

building boundary has been computed, it may be stored and reused easily in the online phase to predict satellite visibility by simply compare the elevation of a satellite with the elevation of the building boundary at the same azimuth.

From the perspective of mobile devices, the algorithm trades time and computing power to a one-off processing requirement at the server side. Specifically, this is achieved by representing the 3D model in a specially designed form - building boundaries at each candidate positions. The logic behind the strategy is that the vast amount of data in a 3D city model is not of direct interest to the shadow-matching algorithm, only where the edges of the buildings are located from a user's perspective matter. Thus, utilizing this knowledge, only building boundaries at each candidate positions are abstracted from the 3D model. This method saves computation load because individual mobile devices do not need to compute the building boundaries on the fly. Instead, they can simply request building boundaries at a certain range of locations, or cache a desired region.

Using stored building boundaries, fewer than fifty comparison and addition operations are required to calculate an overall shadow matching score for one candidate position with two GNSS constellations. Therefore, shadow matching may be performed in real time on a mobile device with several hundred candidate positions, where necessary.

Without any data compression, about 300 bytes are required to store a building boundary with a 1 resolution. If a 2 2 metre grid spacing is used for the candidate positions, a 1 km long 20 m wide street will contain 5000 grid points, requiring 1.5 MB of data storage. By exploiting the similarities both between neighbouring azimuths in the same building boundary and between building boundaries at neighbouring grid points, substantial data compression should be achievable; possibly up to a factor of ten.

Therefore, a standard 4 GB flash drive could store building boundary data for 2500–25000 km of road network. For comparison, the Greater London metropolitan area contains about 15000 km of road. However, as shadow matching is only useful in streets where conventional GNSS positioning is poor, the database need only contain building boundary data for these streets, maybe 10% of the total. Therefore, it should be practical to preload a mobile device with shadow-matching data for several cities, which could be kept up-to-date via the internet.

A software toolkit for generating the grid of building boundaries from a 3D city model was developed in C++. Figure 6 shows the process.
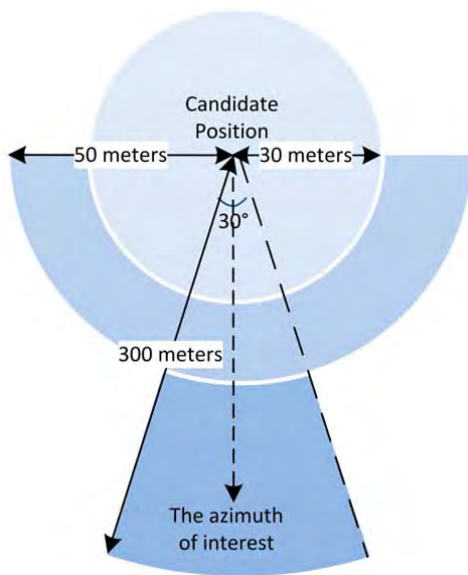
Figure 7 The optimization used in building boundary generation by refining city models according to location of candidate user position and azimuth of interest. (Aerial perspective, the figure is not drawn to scale)

The process can be broken into four steps. Firstly, a one meter by one meter horizontal grid of points, covering the 3D city model area, is generated. The height is set to be 1.5 meters above the terrain height measured in the 3D city model. Secondly, a pre-processing step is developed to eliminate indoor points from the generated grid in the first step, because the current shadow-matching algorithm is designed to work outdoors. Outdoor points are distinguished from indoor ones by testing whether the elevation angle of the sky at each azimuth is 90 degrees. Further details of the algorithms testing line-of-sight visibility can be found in a previous paper (Wang et al, 2012). Thirdly, buildings that are unlikely to block satellite signals are eliminated from the search area, based on checks of their relative location from the candidate position of interest. Finally, the highest elevation angle for a visible sky at each azimuth is tested to determine the building boundary at each outdoor candidate position.

Figure 6 also illustrates the optimization of the process of building boundary generation. Without optimization, it takes an estimated 53 days to perform the process at a 1 m by 1 m grid of candidate positions across a 500 m by 500 m area, using a computer with a CPU speed of 2.67 GHz. In order to improve the efficiency, only buildings that are close to the candidate position and in the direction of interest are tested. Figure 7 illustrates this search area. It should be noted that the parameters used in this example are manually selected based on knowledge of the 3D city model used in this work. Appropriate changes should be made if using another type of city model. After optimization, the time required to generate building boundaries at the same grid of points was reduced to less

than 4 days, a 92.5% reduction in time compared to the original algorithm.

- Step 1 Position Initialization (Online Phase)

In the first step of shadow-matching algorithm, standard point positioning (SPP) using GNSS pseudo-ranges is conducted to acquire an initial user position. In an urban environment, the accuracy is often poor. Consistency checking may be used to identify non-line-of-sight signals and remove them from the position solution (Jiang et al., 2011, Jiang and Groves, 2012). Other available positioning methods (e.g. Wi-Fi or Cell network solution) may be introduced into this step when the GNSS SPP is poor or unavailable.

- Step 2 Determine the Search Area for Candidate Positions from the Building Boundaries at a Grid

The second step defines the search area in which candidate positions are located for the shadow-matching position solution. A search area is defined based on an initial position generated in the first step. A simple implementation can be to draw a fixed-radius circle centred at the initialized position, but more advanced algorithms can be developed to use the knowledge from the initialization process to optimize the search area.

For instance, if the initial position is generated using a conventional GNSS solution, the signal geometry, and hence the positioning accuracy, will be much better along the direction of the street than across the street. This is because an urban canyon affects the geometry of the available GNSS signals. Signals with lines of sight going across the street are much more likely to be blocked by buildings than signals with lines of sight going along the street. Therefore, the conventional GNSS solution has lower accuracy across-street and higher accuracy along-street, which is complementary to shadow-matching algorithm.

Thus, the along-street component of SPP solution can be used as a reference to define the search area and thus generate candidate user positions that vary more in the across-street direction. This is illustrated by the two mobile phones besides the SPP solution in Figure 2, with the green area representing the search area centred at the initial position. A more advanced shadow-matching algorithm would vary the size of its search area based on an assessment of the quality of the SPP solution.

- Step 3 Predict Satellite Visibility at Each Candidate Position

In the third step performed at each candidate position, each satellite's elevation is compared with the building boundary elevation at the same azimuth. The satellite is predicted to be visible if the satellite is above the building boundary.

	Prediction	
	Invisible	Visible
Not tracked	**1**	**0**
Tracked	**0**	**1**

Figure 8: Scoring matrix giving the score for each satellite in shadow matching (SS_{22})

	Prediction		
	Invisible	Diffracted	Visible
Not tracked	**1**	**0.5**	**0**
Tracked	**0**	**0.5**	**1**

Figure 9: Scoring matrix giving the score for each satellite in shadow matching, which models diffraction effects (SS_{23})

	Prediction	
	Invisible	Visible
Not tracked	**1**	**0**
Weak signal (low SNR)	**0.5**	**0.5**
Strong signal (high SNR)	**0**	**1**

Figure 10: Scoring matrix giving the score for each satellite in shadow matching, which account for weak signals that are likely to be caused by signal diffraction and reflection (SS_{32})

	Prediction		
	Invisible	Diffracted	Visible
Not tracked	**1**	**1**	**-1**
Weak signal (low SNR)	**0**	**2**	**0**
Strong signal (high SNR)	**-1**	**1**	**1**

Figure 11: Scoring matrix giving the score for each satellite in shadow matching, which both models diffraction effects and accounts for weak signals that are likely to be caused by signal diffraction and reflection (SS_{33})

Figure 12: Part of the 3D model of London used in the experiments.

The diffraction effect is also modelled in this work (Wang et al., 2012). A three-degree diffraction zone is modelled for building boundaries both horizontally and vertically. Thus, in this model, from the perspective of a GNSS receiver, buildings are three degrees lower and narrower than their actual height and width. If the line-of-sight (LOS) falls within the diffraction region, the signal is predicted to be diffracted. Otherwise, it is predicted to be invisible.

- Step 4: Satellite Visibility Scoring Using Scoring Scheme

For the fourth step, the similarity of the satellite visibility between predictions and observations is evaluated. The candidate positions with the better matches will then be weighted higher in the shadow matching positioning solution. There are two stages for calculating a score for a candidate position. Firstly, each satellite above the elevation mask angle is given a score, calculated based on the predicted and observed visibility, using a scoring scheme. Secondly, the position scoring function, evaluates for each possible user position the overall degree of match between predicted and observed satellite visibility. This is illustrated in (1).

$$f_{pos}(j) = \sum_{i=1}^{n} f_{sat}(i, j, SS) \tag{1}$$

where $f_{pos}(j)$ is the position score for grid point j; $f_{sat}(i, j)$ is the score of satellite i at grid point j; n is the number of satellites above the mask elevation angle; SS is the scoring scheme which defines a score based on predicted and observed satellite visibility.

By the end of this step, each candidate position should have a score to represent the degree to which it matches the observed satellite visibility, and thus how likely it is that each candidate position is close to the true location.

The existing scoring scheme SS_{22} is shown in Figure 8. Only direct line-of-sight (LOS) signals are considered using this scoring scheme, whereas the user equipment can also observe diffracted and reflected signals. This mismatch can degrade shadow-matching performance.

Thus, the scoring scheme has been improved to acknowledge diffraction effects by diffraction modelling. Diffraction occurs at the edge of a building (or other obstacle) when the incoming signal is partially blocked, noting that the path taken by a GNSS signal is several decimetres wide. There are two approaches to predicting the effect of diffraction on satellite visibility using a 3D city model. The first one would be to numerically determine the diffraction field based on every physical factor, including the surface of building, the angle of incidence of the signal and the properties of the GNSS user equipment. This method is impractical because the necessary information about the building materials and antenna characteristics is difficult to obtain and the computational complexity is high. The second, much simpler, approach has been adopted here. This simply extends the building boundary used for satellite visibility determination by adding a diffraction region to model the diffraction effect around building edge. Thus, wherever the LOS intersects the diffraction region, the signal is classified as potentially diffracted instead of blocked (Walker and Kubik, 1996; Bradbury, 2007; Wang et al., 2012). Both horizontal and vertical edges are considered for diffraction modelling. Here, a 3°-wide diffraction region was modelled. The improved scoring scheme SS_{23} as shown in figure 9.

As diffractions and reflections both normally result in weaker signal reception, the signal strength is also built into the new scoring scheme – SS_{32}, as shown in figure 10. In this scheme, a weak signal is regarded likely to be reflected or diffracted, thus it is given a lower weight compared to a strong signal. The boundary to distinguish weak signal from strong signal should be based on the signal to noise ratio (SNR).

Finally, by joining both diffraction modelling and signal strength based scoring, a new SS_{33} scoring scheme is introduced, as shown in figure 11. It should be noted that the scores in these scoring schemes are based on both theory and experimental data. Changes may be needed when using GNSS receivers of other types.

In Section 3, a comprehensive comparison will be conducted to evaluate the influence using different scoring schemes on performance of shadow matching.

• Step 5: Positioning Using Scores at Candidate Positions

The last step of the shadow-matching algorithm is to generate a positioning solution using scores from each candidate position. Shadow matching uses the pattern-matching positioning method (Groves, 2013). As the process of Wi-Fi fingerprinting is similar to the this

process in shadow matching, the algorithms used in Wi-Fi fingerprinting may be investigated for their potential implementation in shadow matching. Potential algorithms include, but are not limited to, k-weighted nearest neighbours, the Bayesian inference received signalstrength (RSS) location method, and the particle filter.

In this work, a method similar to k-nearest neighbours is used to estimate the location, averaging the grid positions of highest scores. With the current scoring system, scores take integer or half-integer values. Therefore, several grid points typically share the highest score. The points in the grid with highest scores are regarded as nearest neighbors. For L nearest neighbors, the location estimate is conducted using (2) and (3) for northing and easting coordinate components:

$$\text{Northing} = \frac{1}{L} \cdot \sum_{i=1}^{L} n_i \qquad (2)$$
$$\text{Easting} = \frac{1}{L} \cdot \sum_{i=1}^{L} e_i \qquad (3)$$

where n_i and e_i are, respectively, the northing and easting coordinates of the ith high-scoring candidate positions. Note that L varies from epoch to epoch depending on how many candidate positions share the highest score.

3. COMPARISON OF VISIBILITY PREDICTION SCORING USING EXPERIMENTAL DATA

The different scoring schemes were tuned and compared using experimental data to improve the accuracy and reliability of shadow matching. Section 3.1 introduces the 3D city model of the Aldgate area of central London, used in the shadow matching experiments. Real-world data sets are collected at sites within the city model area, scattered on major roads and minor roads, at and between junctions. Section 3.2 describes the methods and logics behind implementations of each step of shadow matching. Section 3.3 presents details of selected experimental sites. The experimental results are compared and analysed in Section 3.4 - 3.6.

3.1 City Models

A real 3D city model of the Aldgate area of central London, supplied by ZMapping Ltd, has been used. The model has a high level of detail and decimetre-level accuracy. Figure 12 shows an aerial view of the city model used in this work.

The software toolkit developed for this study stores and processes 3D city model data using Virtual Reality Modelling Language (VRML), an international standard format. Model data in other formats can be transformed to VRML. Buildings in VRML format are represented by structures, which in turn compromise polygons (normally triangle meshes).
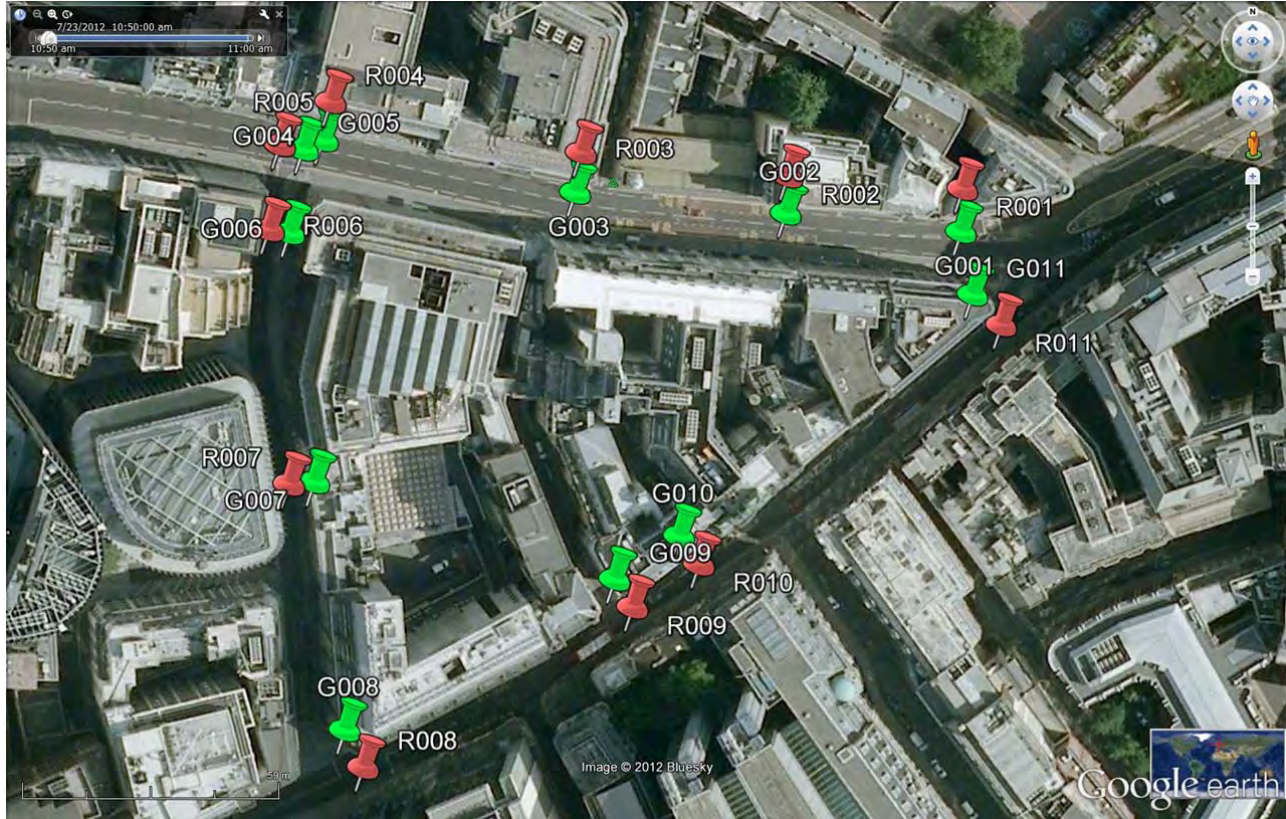
Figure 13: The experimental sites in urban canyons. It shows the experimental sites location in the satellite image in real world.

Figure 14. Left: A photo taken in the experiment on Billiter Street, which is a narrow street. Right: a photo taken in the same experiment on Fenchurch Street.

3.2 Shadow Matching Implementation

In the offline phase, a 1 meter by 1 meter grid has been generated, and the building boundaries determined at each grid point as defined earlier in the paper. They are stored in a specially defined format in a database.

In the online phase, position initialization is not conducted because this study focuses on comparing the different scoring schemes. Different methods used in positioning initialization can result in very different initial positions, so in order to prevent initialization errors from contaminating the following scoring step, the search area for each site is centred at the true position. The search area for each site is defined as everything within a radius of 20 meters, except for the indoor points. Four scoring schemes are deployed at every sites in the satellite visibility scoring step. The modified k-nearest neighbours algorithm is used to determine the positioning solution of shadow-matching algorithm, using (2) and (3).

3.3 Experimental Site Selection

To compare the performance of shadow matching using different scoring schemes, experiments were conducted at 11 pairs of sites, resulting in GNSS data at 22 locations in central London on 23/07/2012. In each pair, two survey-grade GNSS receivers (Leica Viva) were set up on opposite sides of each street (Leadenhall Street, Billiter Street and Fenchurch Street), standing on a footpath close to the traffic lane. GPS and GLONASS observation data were recorded at a 1 Hz rate simultaneously for 10 minutes at each pair of locations. For the purpose of increasing the reliability of the experiments, each site was visited twice at

an interval of approximately 4 hours, allowing the satellite geometry to change completely. The first round is denoted r1, the second round is denoted r2. Thus, in total, 7 hours and 20 minutes of GNSS data was recorded in 44 observation periods at 22 different locations. A summary of the experimental sites is shown in Table 1; their locations are presented in Figure 13. Figure 14 shows two of the narrow streets in the experimental area.

3.4 Signal to Noise Ratio (SNR) Empirical Value

The signal to noise ratio (SNR) is introduced as an indicator of satellite signal quality in the shadow-matching system. An empirical analysis was first conducted to observe the level of SNR in the experimental data. This is because SNR can vary significantly between different types of GNSS receiver. The SNR of the L1 C/A code signal recorded by the Leica Viva GNSS receiver is shown in figures below. Figure 15a shows a period of observations with typical 'strong' SNR values; Figure 15b shows the same period of observation, but with typical 'weak' SNR values. The figure also shows that when the signal is strong, the SNR value typically remains stable (normally around 50 dB-Hz); whereas when the signal is weak, it changes dramatically and the value tends to be lower (normally below 40 dB-Hz).

SNR values of all satellites recorded by two identical Leica Viva receivers in the experimental period show that the SNR mainly ranges between 25 dB-Hz and 55 dB-Hz with an average of 40 dB-Hz. Thus, in those scoring schemes that account for the observed signal quality, signals with SNR > 40 dB-Hz are regarded as strong and signals with SNR ≤ 40 dB-Hz is regarded as weak.

3.5 Score Map of Candidate Positions

At the true position of each experimental site, a 20 meter radius circle is used to generate candidate positions. The pre-calculated candidate grid of building boundaries is loaded in the on-line phase of shadow matching. At each observation epoch, comparison is made between the predicted and observed satellite visibility. Each of the four score schemes is applied to the results for comparison. To illustrate the distribution of scores at the grid points, Figure 16 shows an example of score map for experimental sites G011 (left) and R011 (right).

In Figure 16, the score of candidate positions ranges mainly at the cross-street direction. As G011 and R011 are located at different sides of a street, it is clearly demonstrated that the shadow matching algorithm is sensitive to changes in the across-street direction, but less sensitive in the along-street direction. This is in line with expectations and complements conventional GNSS positioning, which is generally more precise in the along-street direction. There are some spaces that between buildings fall within the search area, but the highest

scoring points are mostly in the correct street. In order to evaluate the performance across all of the experimental data, statistical analysis was conducted.

Table 1. A summary of experimental sites

	1st Round	2nd Round
G001, R001	09:05-09:15	13:07-13:17
G002, R002	09:35-09:45	13:19-13:29
G003, R003	09:10-10:00	13:31-13:41
G004, R004	10:05-10:15	13:44-13:54
G005, R005	10:18-10:28	13:58-14:08
G006, R006	10:33-10:43	14:11-14:21
G007, R007	10:45-10:55	14:23-14:33
G008, R008	10:59-11:09	14:36-14:46
G009, R009	11:14-11:24	14:49-14:59
G010, R010	11:31-11:41	15:03-15:13
G011, R011	11:47-11:57	15:15-15:25
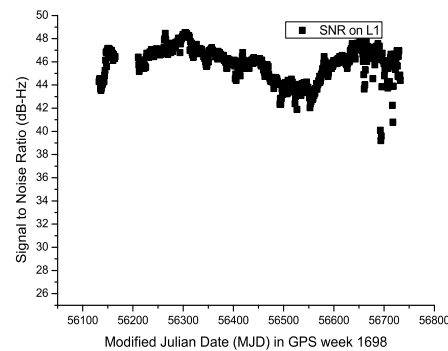
(a)
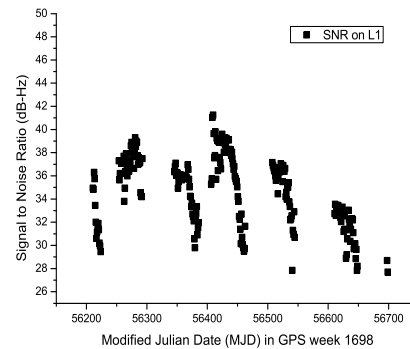
(b)

Figure 15a (top). A period observation of typical strong signal (SNR on L1 of GPS PRN 2, on experimental site ID G001_r1); 15b (bottom). A period observation of typical weak signal (SNR on L1 of GLONASS 18, on experimental site ID G001_r1)
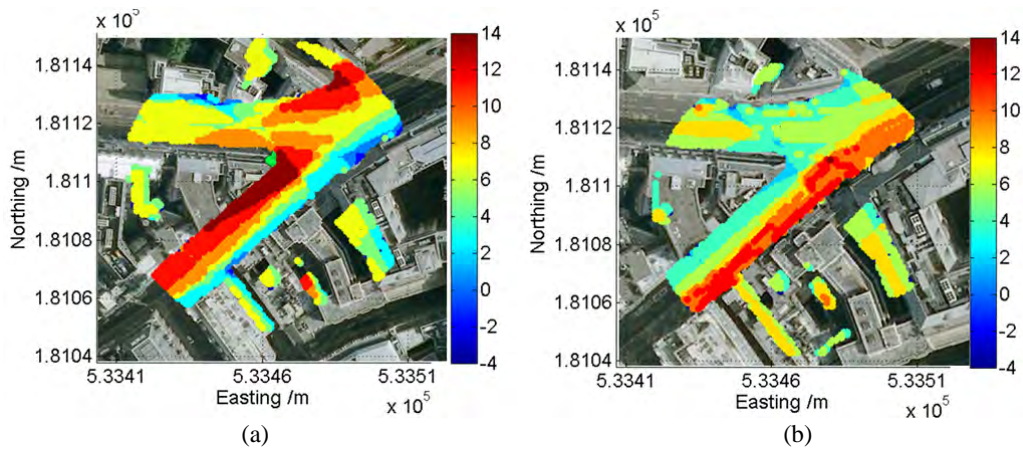
(a)   (b)

Figure 16. Shadow-matching score map of experimental sites G011 (a) and R011 (b) using 3x3 scoring scheme SS_{33} (at epoch 11:55:40 23 July 2012). The circles represent the candidate positions. The red bar is where the shadow-match positioning solution is. Refer to Figure 13 for the true location of each site. For illustration purposes, a 50 meter-radius circular search area centered at each truth position is used.
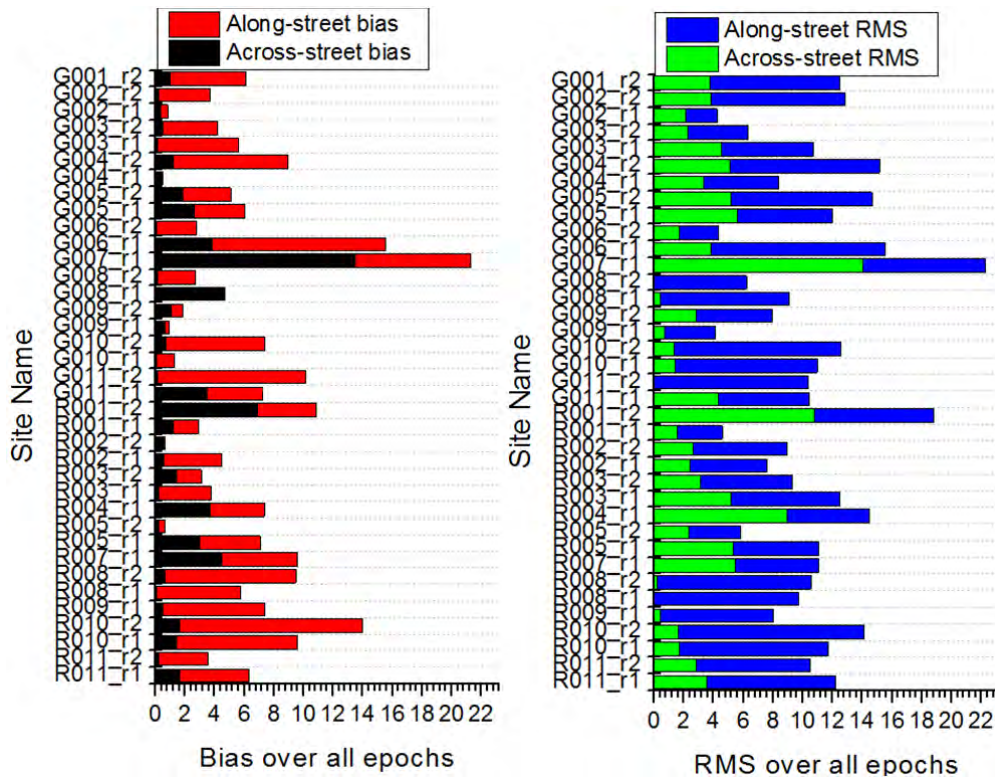

Figure 17. The average bias and RMS between shadow matching positioning solution from true position for each experimental sites using the 2 * 2 scoring matrix.
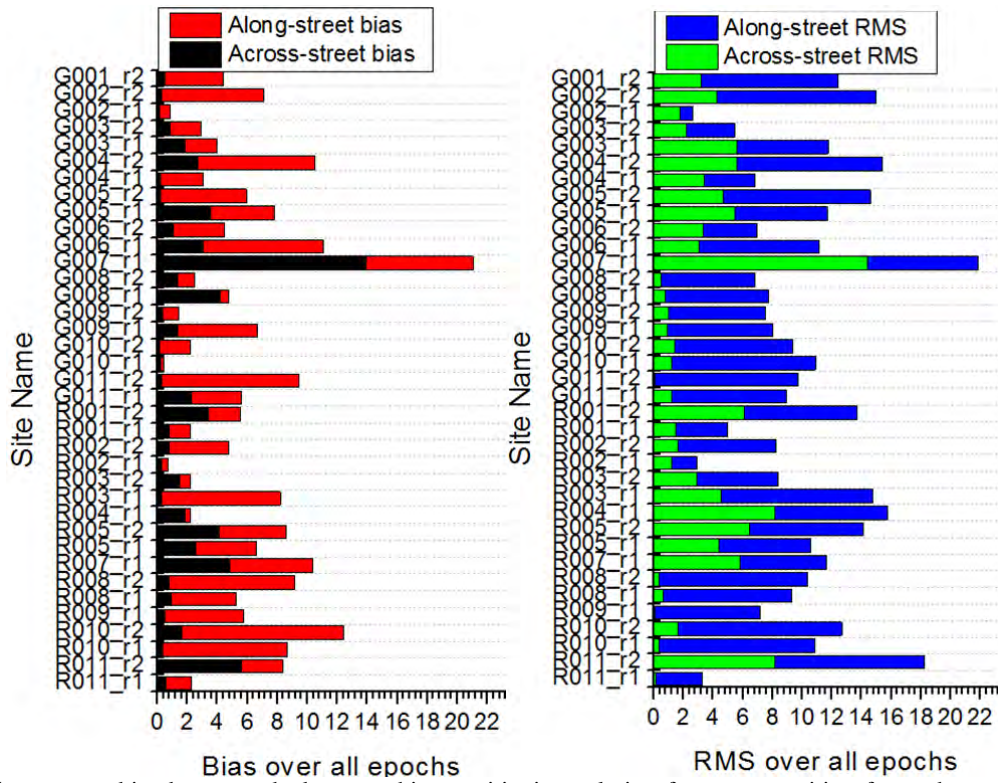
432

Figure 18. The average bias between shadow matching positioning solution from true position for each experimental sites using the 2 * 3 scoring matrix.
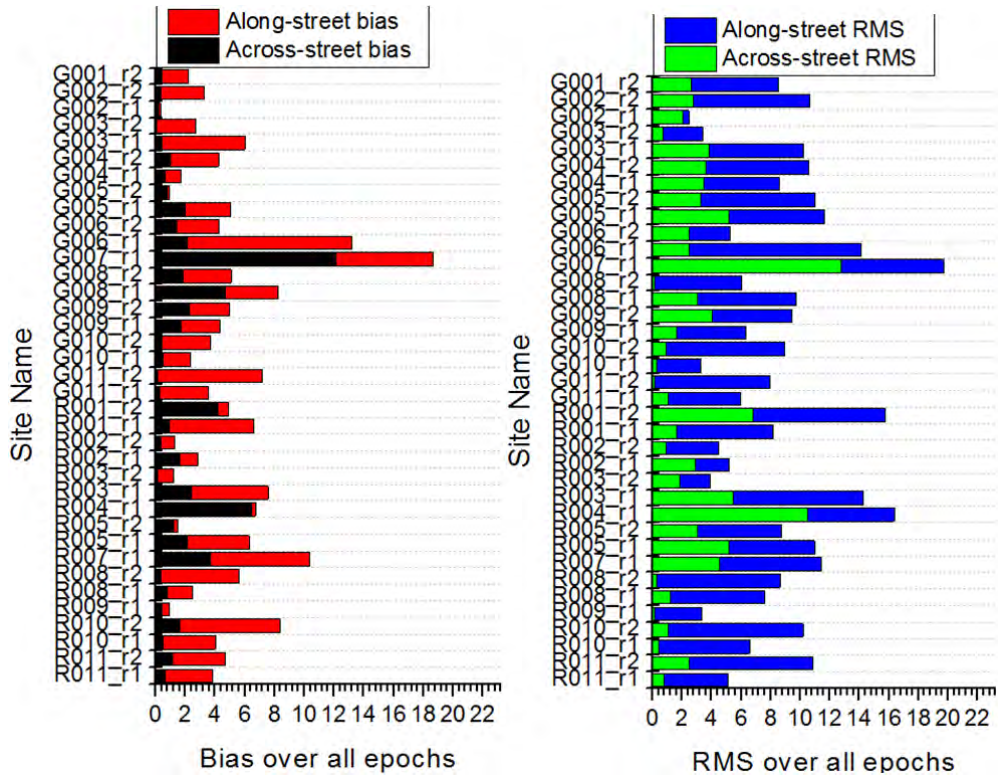

Figure 19. The average bias between shadow matching positioning solution from true position for each experimental sites using the 3 * 2 scoring matrix.
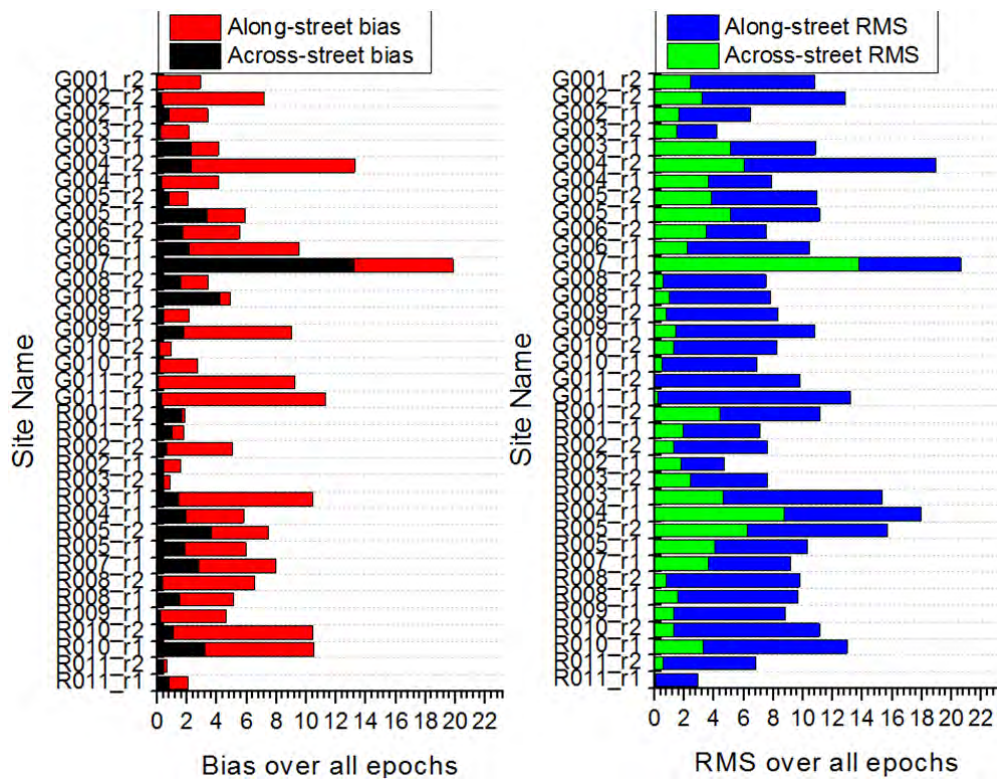
Figure 20. The average bias between shadow matching positioning solution from true position for each experimental sites using the 3 * 3 scoring matrix.

3.1 Statistical Analysis

Two indicators, average bias and root mean square error (RMS), are used for each experimental site to evaluate the performance of shadow matching. The bias is transformed from local coordinates (Northing and Easting) to the along-street and across street direction. In order to compare shadow matching using the different scoring schemes, the average biases and RMS at each site are compared in Figures 17 - 20, noting that the statistics cover a 10 min observation period, during which the constellation geometry changes slowly, so the results are highly correlated over time. The y-axis is in meters. Where separate statistics are calculated for the two different observation periods at the same site, results for which may be considered independent. A few sites are missing from the results because fewer than four satellites were observed so an SPP solution could not be computed and the GNSS receivers used for this experiment would not record the measurement due to the design of their software.

It is shown in Figure 17 - 20 that the along street average bias is typically higher than the across street one. As shadow matching was designed to improve the cross-street positioning, and may be combined with conventional GNSS and other possible techniques, this is not considered to be a problem.

Further statistics have been computed to average the bias and RMS error using each scoring scheme, the results are shown in Figure 21. Similarly, Figure 22 also compares

different scoring schemes for their effects on shadow matching performance in terms of success rate of positioning error with certain meters. It can be seen from both graphs that different scoring schemes have a relatively small influence on the performance of shadow matching, which means the shadow matching performance is not very sensitive to the scoring schemes. However, there is a small improvements using the new SS_{33} scoring scheme. For example, in Figure 21, the new scoring scheme improves the cross street accuracy with an average bias of 1.61 m, with a 9.4% reduction compared to the original SS_{22} scoring scheme. Similarly, the cross street RMS is 2.86 m, a reduction of 15.3%.

As the street is around 10 meters wide, a positioning accuracy better than 5 meters is considered good enough to determine the correct side of the street, while a positioning accuracy better than 2 meters is considered good enough to distinguish the foot path from a traffic lane. Figure 20 shows success rate in terms of achieving a cross-street error within 1, 2, 3, 4, and 5m. It shows that the success rate for determining the correct side of a street is 89.3%, 3.6% better than using the previous SS_{22} scoring scheme; the success rate of distinguishing the footpath from a traffic lane is 63.6% of the time, 6.8% better than using the previous SS_{22} scoring scheme.
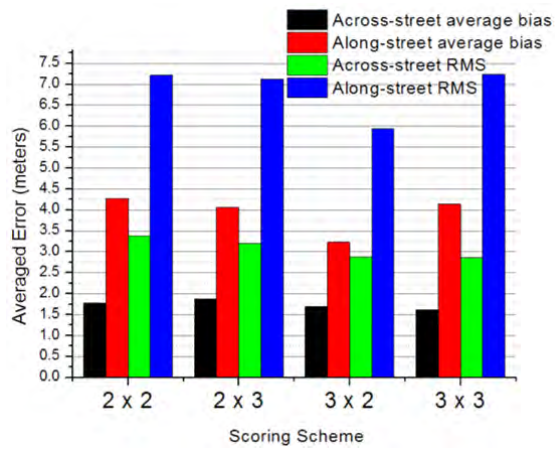
Figure 21. The average bias and RMS that is averaged between all experimental sites, using different scoring matrix in shadow matching algorithm.
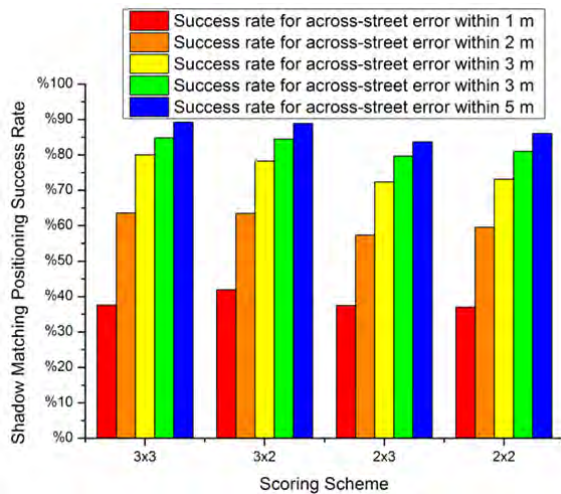

Figure 22. The success rate of positioning error using shadow matching in cross-street direction.

4 CONCLUSION AND FUTURE WORK

In this work, four contributions have been made. Firstly, a new scoring scheme, a key element of the algorithm to weight candidate user locations, is proposed. The new scheme takes account of the effects of satellite signal diffraction and reflection by weighting the scores based on diffraction modelling and signal-to-noise ratio (SNR). Furthermore, an algorithm similar to k-nearest neighbours (k-NN) is developed to interpolate the position solution over an extensive grid. The process of generating this grid of building boundaries is also optimized. Finally, instead of just testing at two locations as in the earlier work, real-world GNSS data has been collected at 22 different locations in this work, providing a more comprehensive and statistical performance analysis of the new shadow-matching algorithm.

Figure 23. Conventional GNSS positioning solution using weighted least square (WLS) at site G003.

In the experimental verification, the new scoring scheme achieves an average cross street accuracy to 1.61 m, a 9.4% improvement over the previous scheme, while the cross street RMS error is 2.86 m, a 15.3% improvement. Figure 22 shows that the success rate for determining the correct side of a street is 89.3%, a 3.6% improvement, while the success rate for distinguishing the footpath from a traffic lane is 63.6%, a 6.8% improvement.

Conventional GNSS positioning performs relatively poorly in the across street direction, and better along the street. Figure 23 shows the conventional GNSS positioning solution at point G003_r1 using weighted least square (WLS). It demonstrates that the cross street position from the conventional GNSS solution can vary by 40 meters. As shadow matching has a cross-street accuracy of a few meters, it is highly complementary to conventional GNSS positioning methods.

In future work, shadow matching using GPS and GLONASS data from a smartphone will be tested. Four-constellation shadow-matching performance will also be predicted by combining GPS and GLONASS data from two different epochs, separated in time. The Bayesian inference received signal strength (RSS) location method, and the particle filter may be investigated for the shadow matching positioning algorithm. Further investigations will be conducted to improve the shadow-matching algorithm.

To obtain an accurate and reliable position solution in challenging urban environments, shadow matching must be combined with conventional GNSS positioning, NLOS signal detection and other techniques that exploit the 3D mapping, such as height aiding. This concept is known as intelligent urban positioning (IUP) and is introduced in Groves et al (2012b). IUP may also be extended to incorporate other techniques, such as Wi-Fi, Bluetooth Low Energy, and MEMS inertial sensors.

ACKNOWLEDGEMENTS

REFERENCES

BRADBURY, J, Prediction of Urban GNSS Availability and Signal Degradation Using Virtual Reality City Models. Proceedings of the 20th International Technical Meeting of the Satellite Division of The Institute of Navigation (ION GNSS 2007), September 25 - 28 2007 Fort Worth, TX. 2696 - 2706.

BRADBURY, J., ZIEBART, M., CROSS, P. A., BOULTON, P. & READ, A, 2007. Code Multipath Modelling in the Urban Environment Using Large Virtual Reality City Models: Determining the Local Environment. The Journal of Navigation, 60, 95-105.

BROLL, W., I. Lindt, I.Herbst, J.Ohlenburg, A. K. Braun and R. Wetzel (2008), 'Toward next-gen mobile AR games', Computer Graphics and Applications, IEEE 28(4), 40-48.

BRUNER, J, 2008. Greening the Traffic Lights. Forbes Magazine May 05 2008; Available from: http://www.forbes.com/forbes/2008/0505/064.html.

ERCEK, R., DONCKER, P. D. & GRENEZ, F, Study of Pseudo-Range Error Due to Non-Line-of-Sight-Multipath in Urban Canyons. Proceedings of the 18th International Technical Meeting of the Satellite Division of The Institute of Navigation (ION GNSS 2005), September 13 - 16 2005 Long Beach, CA 1083 - 1094.

FARRELL, J. A, 2008. Aided navigation: GPS with high rate sensors, McGraw-Hill Professional.

GROVES, P. D., 2008. Principles of GNSS, Inertial, and Multisensor Integrated Navigation Systems, First Edition, Boston, London, Artech House.

GROVES, P. D, 2011. Shadow Matching: A New GNSS Positioning Technique for Urban Canyons The Journal of Navigation.

GROVES, P. D., WANG, L. & ZIEBART, M (2012a). Shadow matching: Improved GNSS accuracy in Urban canyons, GPS World, 23(2), 14 - 18+27-29.

GROVES, P D, JIANG, Z., WANG, L., ZIEBART, M. (2012b). Intelligent Urban Positioning using Multi-Constellation GNSS with 3D Mapping and NLOS Signal Detection, *Proceedings of the 25th International Technical Meeting of The Satellite Division of the Institute of Navigation (ION GNSS 2012)*, Nashville, Tennessee, September 2012.

GROVES, P.D., 2013, Principles of GNSS, Inertial, and Multi-Sensor Integrated Navigation Systems, Second Edition, Boston, London, Artech House, to be published in 2013.

JI, S., CHEN, W., DING, X., CHEN, Y., ZHAO, C. and HU, C. (2010). Potential Benefits of GPS/GLONASS/GALILEO Integration in an Urban Canyon – Hong Kong. The Journal of Navigation, 63, 681–693.

JIANG, Z., GROVES, P., OCHEING, W. Y., FENG, S., MILNER, C. D. & MATTOS, P. G, Multi-Constellation GNSS Multipath Mitigation Using Consistency Checking. ION GNSS 2011, September 19-23 2011 Oregon Convention Center, Portland, Oregon.

JIANG, Z, GROVES, P D, "GNSS NLOS and Multipath Error Mitigation using Advanced Multi-Constellation Consistency Checking with Height Aiding," *Proceedings of the 25th International Technical Meeting of The Satellite Division of the Institute of Navigation (ION GNSS 2012)*, Nashville, Tennessee, September 2012.

KIM, H. I., PARK, K. D. and LEE, H. S. (2009). Development and Validation of an Integrated GNSS Simulator Using 3-D Spatial Information. Journal of the Korean Society of Surveying Geodesy Photogrammetry and Cartography, 27, 659–667.

OMER, R, COULTON P, and EDWARDS, R. (2005) *Implementing Location Based Information/Advertising for Existing Mobile Phone Users in Indoor/Urban Environments.* In: Mobile Business, 2005. ICMB 2005. IEEE, pp. 377-383. ISBN 0-7695-2367-6

SUH, Y. and SHIBASAKI, R. (2007). Evaluation of satellite-based navigation services in complex urban environments using a three-dimensional GIS. *IEICE Transactions on Communications*, *E90-B*, *1816–1825*.

VIANDIER, N., NAHIMANA, D. F., MARAIS, J. & DUFLOS, E, Gnss performance enhancement in urban environment based on pseudo-range error model. Position, Location and Navigation Symposium, 2008 IEEE/ION, 5-8 May 2008 2008. 377-382.

WALKER, R. & KUBIK, K. 1996. Numerical Modelling of GPS Signal Propagation. Proceedings of the 9th International Technical Meeting of the Satellite Division of The Institute of Navigation (ION GPS 1996). Kansas City, MO

WANG, L., GROVES, P. & ZIEBART, M. (2011). GNSS Shadow Matching Using A 3-D Model of London. *Proceedings of the European Navigation Conference*, Grange Tower Bridge, London.

WANG, L., GROVES, P. D. & ZIEBART, M (2012). Multi-Constellation GNSS Performance Evaluation for Urban Canyons Using Large Virtual Reality City Models.

Journal of Navigation, 65, pp 459-476 doi:10.1017/S0373463312000082.

YOU, Yilun, TAT Jun Chin, JOO Hwee Lim, Jean-Pierre Chevallet, Line Coutrix and Laurence Nigay (2008), 'Deploying and evaluating a mixed reality mobile treasure hunt: Snap2play'. MobileHCI '08, Proceedings of the 10th international conference on Human computer interaction with mobile devices and services, pp 335-338.